# Blends of AB/BC Diblock Copolymers with a Large Interaction Parameter $\chi$

**H. Frielinghaus***

*Forschungszentrum Jülich GmbH, IFF, D-52425 Jülich, Germany*

**N. Hermsdorf**

*Institut für Polymerforschung Dresden, D-01069 Dresden, Germany*

**R. Sigel**

*Max-Planck-Institut für Kolloid und Grenzflächenforschung, D-14424 Potsdam, Germany*

**K. Almdal and K. Mortensen**

*Risø National Laboratory, Danish Polymer Center, DK-4000 Roskilde, Denmark*

**I. W. Hamley**

*School of Chemistry, University of Leeds, Leeds LS2 9JT, UK*

**L. Messé, L. Corvazier, and A. J. Ryan**

*Dept of Chemistry, University of Sheffield, Sheffield S3 7HF, UK*

**D. van Dusschoten and M. Wilhelm**

*Max-Planck-Institute for Polymer Research, D-55021 Mainz, Germany*

**G. Floudas and G. Fytas**

*Institute of Electronic Structure and Laser, GR-71110 Heraklion, Greece*

*Received February 8, 2001*

ABSTRACT: Blends of poly(styrene)-*b*-poly(isoprene) (PS−PI) and poly(isoprene)-*b*-poly(ethylene oxide) (PI−PEO) were investigated by small-angle X-ray scattering, photon correlation spectroscopy, light microscopy, and rheology. Blends were prepared in which both diblocks had the same PI composition, *f*, and were investigated as a function of blend composition, Φ. We generally found a disordered one-phase region at high temperatures and two macrophase-separated, ordered phases at low temperatures. At low temperatures the only appreciable miscibility was found for $f = 0.7$ in the PI−PEO-rich phase. At intermediate temperatures we generally observed macrophase separation before microphase separation upon cooling. The macrophase separation boundary compared to the microphase boundary is lowered upon increasing *f*. For $f = 0.6$ and 0.7 we observe an adjustment of the *d* spacing of the macrophase-separated, ordered phases. The general trend of the phase behavior is described by a theory using the random phase approximation.

## Introduction

Polymers are generally immiscible at low temperatures, and phase separation occurs in blends. The phase-separated domains can evolve up to macroscopic dimensions (∼1 $\mu$m or more), and so the process is termed macrophase separation. The enthalpic demixing that occurs in block copolymers at low temperatures, on the other hand, leads to microphase separation, because the blocks are tethered together, preventing macrophase separation. The result is an ordered structure with a period ∼5−100 nm. The interplay between macro- and microphase separation has been investigated for blends of one homopolymer with a block copolymer, two homopolymers with a block copolymer, and also blends of block copolymers.[1]

In this paper, we investigate the phase diagrams of blends of two different, strongly interacting, diblock copolymers. The interaction between the blocks is mediated by using a common block B; i.e., we consider AB/BC blends. We identify regions of macro- and microphase separation via a combination of small-angle scattering techniques and rheology. Blends containing a poly(styrene)-*b*-poly(isoprene) diblock and a poly(isoprene)-*b*-poly(ethylene oxide) diblock were prepared in which both diblocks had the same composition, *f*. Blends of symmetric diblocks ($f = 0.5$) and asymmetric diblocks ($f = 0.6$ and $f = 0.7$) were investigated as a function of blend composition (Φ).

The phase behavior of blends of chemically identical diblocks (AB/AB blends) has been investigated in detail for both symmetric diblocks and asymmetric diblocks.[1] In particular, Hashimoto and co-workers have studied the morphology of blends of PS−PI diblocks via transmission electron microscopy and small-angle X-ray scattering.[2−4] Qualitatively, the results can be summarized according to the molecular weight ratio of the two diblocks; if this is less than five, then the two diblocks were found to be miscible, whereas if it was greater than 10, the copolymers showed partial

10.1021/ma010233q CCC: $20.00 
Published on Web 06/09/2001

miscibility or macrophase separation depending on the blend composition.[5] A number of other reports on the morphology of AB/AB blends have appeared. [1,6−8]

A prime reason to investigate blends of block copolymers, and the motivation for the present research, is the possibility to prepare morphologies that differ from those in the constituent diblocks. In the case of AB/BC diblocks there exists the exciting possibility to prepare, simply by judicious blending of diblocks, complex morphologies of the type observed for ABC triblock copolymers, which are difficult to synthesize with precise control of composition. We are aware of only one previous report on the morphology of AB/BC blends. Kimishima et al.[9] examined blends of poly(styrene)-*b*-poly(ethylene propylene) (PS−PEP) and poly(styrene)-*b*-poly(isoprene, partially hydrogenated) (PS−HPI) prepared by solvent casting. They reported a lamellar morphology of alternating PS and mixed PEP/HPI domains as the initial microphase-separated structure during the solvent casting process. For low degrees of hydrogenation (higher immiscibility) macrophase separation occurred following the initial microphase separation. However, when the extent of hydrogenation of the PI was sufficiently high, microphase separation occurred between HPI and PEP, leading either to a modulated structure within the rubbery lamellae or to segregation of PEP and HPI lamellae. However, these intermediate structures were only observed as trapped nonequilibrium morphologies due to the solvent casting process. It thus remains an open question whether complex, and even novel, morphologies can be created by blending AB and BC diblocks. In AB/AB blends, however, evidence has been presented for an unidentified (bicontinuous) nonlamellar morphology in a blend of lamellar-forming diblocks.[2]

From a theoretical viewpoint, phase separation in AB/BC blends has been modeled using mean-field theory and the random phase approximation.[10] Self-consistent-field theory has been applied to mixtures of chemically identical diblocks (references are contained in ref 1) but not to our knowledge to blends of dissimilar diblocks.

This paper is organized as follows. Mean-field theory used to model the phase boundaries is outlined qualitatively in the next section (full details are contained in ref 10). Then results are presented, primarily from small-angle scattering experiments, that lead to phase diagrams showing macro- and microphase separation transition lines. Rheology and light microscopy provide information on phase transition temperatures and phase-separated morphologies, respectively. In addition, the dynamics of the blend are probed via photon correlation spectroscopy. Finally, our results are summarized.

## Theory

The theory of Olmsted and Hamley[10] predicts the phase diagrams of AB/BC block copolymer blends within mean-field theory. This theory is based on the principles already derived elsewhere.[11] The fluctuation modes are treated within the random phase approximation. Depending on the length scale $\lambda$ (related to the scattering vector by $q = 2\pi/\lambda$) of the critical fluctuation mode, macrophase or microphase separation can be distinguished. Whereas phase separation into two macroscopic phases means a separation into AB- and BC-rich phases at large length scale ($q = 0$), the microphase ordering is due to the covalent bond between the two blocks, which prevents the separation on large length scales. The aim of the original theory work[10] was to determine Lifshitz points, which result from the competition between macrophase and microphase separation. In this paper we want to use the theory in order to compare experimental data with the general features expected for the phase diagrams. Limitations of this theory are due to (a) the negligence of strong fluctuations, which make the theory only semiquantitative, and to (b) the possibility of only describing the first phase boundary limiting the one-phase, disordered state. This means that for a certain set of ($f$,$\Phi$) values the phase boundary of highest temperature can be considered correctly only. However, if discussing a macrophase separation dominated phase diagram, the two separated phases still obey thermodynamic rules and therefore their microphase separation is described by the same principles; i.e., we can use the same theory within our approximation. The reversed case, i.e., a microphase separation dominated phase diagram, makes the discussion of macrophase separation questionable. Here we display the calculated macrophase separation boundary just for demonstration. A one-phase ordered diblock copolymer melt, which crosses a macrophase separation phase boundary, would be hindered to relax due to the ordered structures anyways.

**Table 1. Diblock Copolymers Studied**

| sample (b1−b2-no.) | $M_n$ (stoich) [$10^3$ g/mol] | $M_w$ (GPC) [$10^3$ g/mol] | $M_w/M_n$ (GPC) | $f_{PI}$ | $T_{ODT}$ [K] |
|---|---|---|---|---|---|
| PS−PI-1 | 17.0 | 20.7 | 1.03 | 0.46 | 390 |
| PS−PI-2 | 24.5 | 28.9 | 1.04 | 0.44 | 473 |
| PS−PI-3 | 20.4 | 18.1 | 1.04 | 0.73 | |
| PS−PI-4 | 30.0 | 30.3 | 1.02 | 0.73 | 437 |
| PS−PI-5 | 24.9 | 24.4 | 1.04 | 0.53 | 479 |
| PS−PI-6 | 17.0 | 21.9 | 1.10 | 0.58 | 443 |
| PS−PI-7 | 21.0 | 22.0 | 1.09 | 0.58 | 443 |
| PI−PEO-1 | 4.0 | 4.4 | 1.06 | 0.50 | 405 |
| PI−PEO-2 | 5.7 | 7.4 | 1.10 | 0.49 | 520 |
| PI−PEO-3 | 7.3 | 8.2 | 1.05 | 0.70 | 509 |
| PI−PEO-4 | 6.7 | 7.2 | 1.06 | 0.60 | 497 |

We have previously used this theory to predict phase diagrams using interaction parameters determined experimentally. Results of small-angle scattering experiments for a blend of symmetric ($f = 0.5$) diblock copolymers PS−PI-1/PI−PEO-1 (Table 1) were discussed.[12] The system has the one-phase, disordered state at high temperatures. Upon cooling, macrophase separation into two disordered phases is predicted to occur. Figure 1a shows the binodal and the spinodal line, meeting at the critical point. Upon further cooling, the two phases order independently. Only at very low or high concentrations of PI−PEO, a direct transition from the one-phase, disordered state to the one-phase, ordered state can be expected. Therefore, the phase diagram is dominated by macrophase separation.

The predicted phase diagram (Figure 1b) of the PS−PI-6/PI−PEO-4 blend with a slightly longer PI-block ($f \approx 0.6$) exhibits for PI−PEO-rich samples a one-phase, ordered state first. For intermediate compositions the macrophase separation dominates. The competition between macrophase and microphase separation makes the phase diagram looking similar to one containing a Lifshitz point. However, the microphase spinodal has not exactly reached the critical point of macrophase separation, as it would in the case of a Lifshitz point. At very low PI−PEO compositions the microphase separation dominates again.

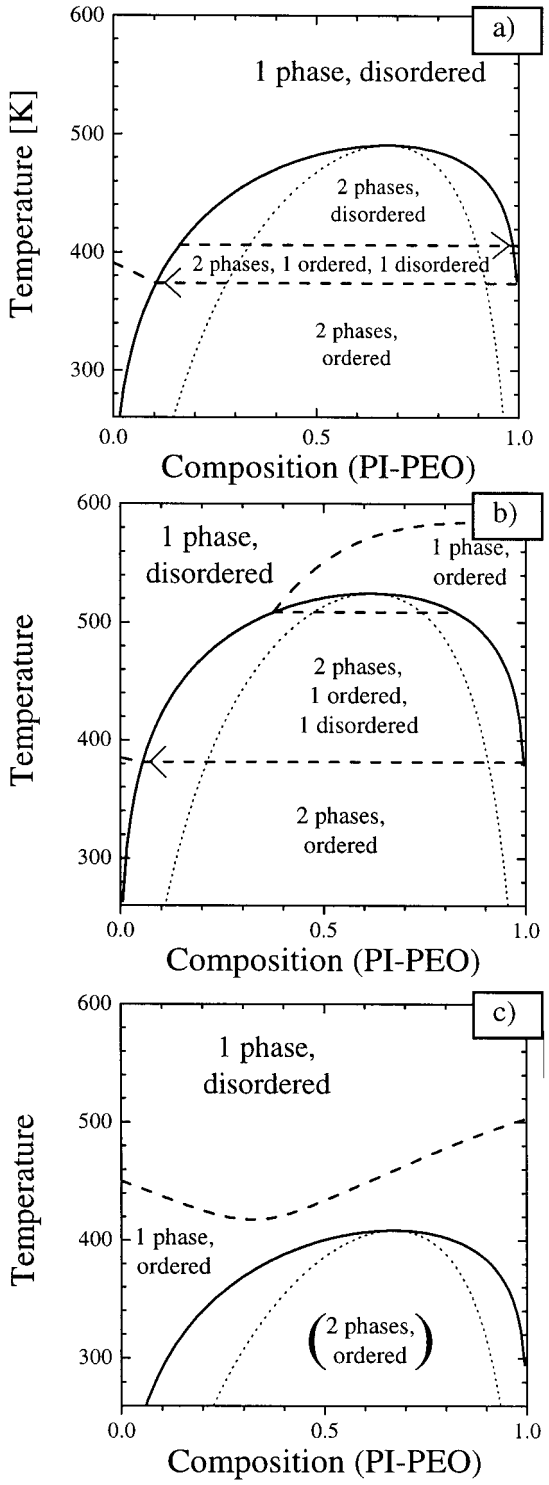


**Figure 1.** (a) Predicted phase diagram for a PS−PI-1/PI−PEO-1 blend with the chain length ratio $f = 0.5$. The phase diagram is dominated by macrophase separation. The corresponding binodal (solid line) and spinodal (dotted line) meet in the critical point. The separated phases are predicted to microphase separate (i.e., order) independently. The corresponding spinodal is depicted by a dashed line. (b) Predicted phase diagram for a PS−PI-6/PI−PEO-4 blend with the chain length ratio $f = 0.6$. The phase diagram is dominated by partially microphase and partially macrophase separation. The line types are the same as in (a). (c) Predicted phase diagram for a PS−PI-4/PI−PEO-3 blend with the chain length ratio $f = 0.7$. The phase diagram is dominated by microphase separation. The line types are the same as in (a).

The predicted phase diagram (Figure 1c) of the PS−PI-4/PI−PEO-3 blend with the longest PI-block ($f \approx 0.7$) indicates a transition from the one-phase, disordered state at high temperatures to the one-phase, ordered state. Thus, this phase diagram is dominated by microphase separation.

In summary, the three examples describe the transition from a macrophase separation dominated to a microphase separation dominated phase diagram by varying the copolymer composition $f$ (holding the molecular weights approximately constant). Close to $f = 0.6$, a first-order Lifshitz point is approached. Within the given uncertainties of the interaction parameter determination, the molecular weight, and due to the restriction to the random phase approximation, we do not present more precise coordinates of the Lifshitz point here. The suppression of the macrophase separation was already speculated by just discussing the effective interaction parameter $\chi_{macro}$ in ref 12.

## Synthesis and Sample Preparation

Poly(isoprene)-*b*-poly(styrene) (PI−PS) and poly(isoprene)-*b*-poly(ethylene oxide) (PI−PEO) diblock copolymers were synthesized by anionic polymerization using established procedures.[13] The polymerization was carried out at 313 K using *sec*-butyllithium as the initiator and cyclohexane as the solvent for PI−PS and hydroxy-functionalized PI (PI−OH). These conditions lead to atactic polystyrene and a high degree of 1,4-addition of isoprene (75% cis-1,4; 20% trans-1,4; 5% 3,4-addition). Poly(isoprene)-*b*-poly(ethylene oxide) diblock copolymers were synthesized by anionic polymerization in the solvent tetrahydrofuran (THF) at 313 K from PI−$O^-$ as the initiator, prepared from PI−OH with naphthylpotassium. The compositions of the diblock copolymers were calculated from the masses of the added monomers; the yield was greater than 98% in all cases. The volume fraction of poly(isoprene) $f_{PI}$ was estimated using the densities 1.06, 0.97, and 0.83 g $cm^{-3}$ for PEO, PS, and PI at 413 K, respectively. All of the synthesized diblock copolymers had a relatively narrow polydispersity ($M_w/M_n < 1.07$), which was determined by size exclusion chromatography. This method also provided a relative measure of the overall molecular weight and confirmed the absence of homopolymer.

**Materials.** Ethylene oxide (Air Liquide) was dried over $CaH_2$ and cryo-distilled into an ampule. *sec*-Butyllithium (Aldrich, 1.3 M in cyclohexane), acetic acid, methanol, and dibutylmagnesium (Aldrich, 1.0 M in heptane) were used without further purification. Cyclohexane was freshly distilled, and THF was distilled from sodium metal in the presence of benzophenone under argon. Isoprene (Aldrich) and Styrene (Fluka) were cryo-distilled twice, first from $CaH_2$ and then from dibutylmagnesium directly into an ampule. Reactions were performed on a vacuum line. The apparatus was dried by several heating and evacuation cycles and flushed with argon. Naphthylpotassium was synthesized following an established procedure[14] and stored at room temperature.

**Polymerization of Diblock Copolymer Poly(isoprene)-*b*-poly(ethylene oxide).** Freshly distilled cyclohexane was cooled in an ice bath, and isoprene was introduced from an ampule. After addition of *sec*-butyllithium, the reaction mixture was stirred for 30 min. After heating to 313 K the mixture was stirred for 4 h at this temperature. After addition of a 15-fold excess of ethylene oxide compared to the initiator concentration to cap the living PI chain ends, the

mixture was stirred for another 30 min. The reaction was quenched with acetic acid, and the solvent was removed under vacuum. The polymer was dissolved in chloroform and extracted with water. Then the polymer was dried under vacuum and was finally obtained as colorless oil. The PI−OH was transferred into a glass reactor and further dried under high-vacuum conditions overnight. After dissolution in freshly distilled THF, the solutions were titrated with deep green naphthylpotassium solution. The addition of naphthylpotassium was stopped after a green color remained for at least 5 min. Ethylene oxide was added and polymerized for at least 2 days at 313 K. The reaction was terminated with acetic acid, and the potassium acetate was removed by dissolving the polymer in chloroform and extracting the salt with a $Na_2CO_3$ solution. Finally, the polymer was dried under vacuum, dissolved in toluene, and precipitated in cold acetone.

**Polymerization of Diblock Copolymer Poly(isoprene)-*b*-poly(styrene).** Styrene was introduced from an ampule into a flask containing freshly distilled cyclohexane. After addition of *sec*-butyllithium, the reaction mixture was stirred for 2 h at 313 K. The solution was cooled to 273 K, and isoprene was introduced from an ampule. The reddish color disappeared immediately. The reaction mixture was stirred for 30 min, and after heating to 313 K the mixture was stirred another 4 h at this temperature. Subsequently, the reaction was quenched with methanol. The polymer was precipitated in methanol and collected as a white powder, which was dried under vacuum.

**Solvent Casting.** The blends of two diblock copolymers with identical PI compositions $f$ (Table 1) were prepared by dissolving the components together in chloroform and drying them under high-vacuum conditions. In this paper we discuss the three blends ofPS−PI-1/PI−PEO-1, PS−PI-6/PI−PEO-4, and PS−PI-4/PI−PEO-3, in which both diblocks had the same PI-content $f$.

## Experimental Section

**Small-Angle X-ray Scattering (SAXS).** Experiments were performed on beam line 8.2 at the Synchrotron Radiation Source, Daresbury Lab, UK. Details of the storage ring, radiation ($\lambda = 1.5$ Å), camera geometry, and the data collection electronics have been given elsewhere.[15] The camera was equipped with a multiwire quadrant detector at a distance of 3.5 m from the sample position. The sample was prepared in a DSC pan (fitted with Mica windows of 7 mm diameter), which was placed in the spring loaded holder of a Linkam TMH600 hot stage. The data were corrected for background scattering, sample absorption, and the positional alinearity of the detector. The scattering data are presented as a function of the wavenumber $q = 4\pi/\lambda \sin\theta$, where $2\theta$ is the scattering angle.

**Photon Correlation Spectroscopy (PCS).** The intermediate scattering function $C(q,t)$ of the diblock copolymer blend PS−PI-1/ PI−PEO-1 with volume fraction of the PI−PEO diblock, $\Phi = 0.7$, was obtained from the intensity correlation function $G(q,t)$:

$$C(q,t) = [(G(q,t) - 1)/f'] \quad (1)$$

over the temperature range 408−445 K. In eq 1, $f'$ is an instrumental factor and the experimental $G(q,t)$ was measured using an ALV-5000 digital correlator. The intensity $I_c$ associated with the relevant concentration fluctuations at low wavevectors $q$ is computed from the total light scattering

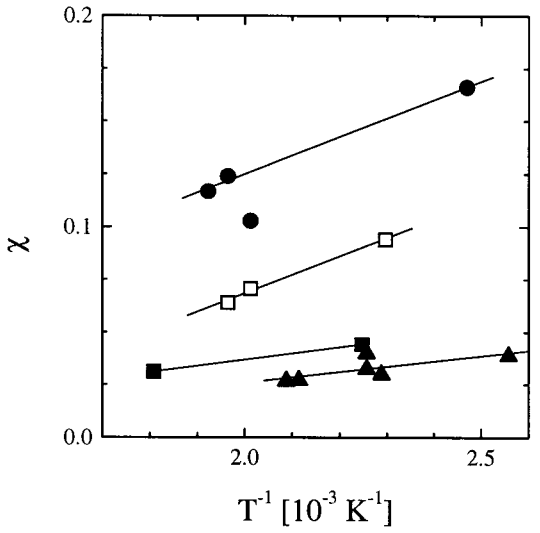


**Figure 2.** Experimental Flory−Huggins interaction parameter $\chi$ as a function of the inverse temperature. The single data points result from PI−PEO (●), PS−PI (▲), and PS−PEO (■) diblock copolymers and PS/PEO (□) homopolymer blends. The solid lines are linear fits to early synthesized samples and have been published in ref 12.

$I_c(q)$ and the amplitude α of $C(q,t)$ due only to $I_c$. In the presence of additional processes the correct $I_c$ is accessible in a dynamic experiment. In fact, as shown in Figure 7, two processes contribute to $C(q,t)$ at high temperatures.

**Light Microscopy (LM).** Images were obtained with a Nikon Optiphot polarization microscope with an attached camera. An overall magnification of 20× to 160× could be achieved. The sample was placed on a glass slide and covered by a coverslip. A Mettler FP82HT hot stage allowed for in situ heating and cooling experiments with a constant magnification of 20×. A continuous nitrogen flow prevented oxidation. We typically used heating and cooling rates of 10 K/min and stopped at certain temperatures for photography. Using crossed polars, it was possible to observe the crystallization of the PEO but not to observe further birefringence of ordered diblock copolymer phases.

**Rheology.** Dynamic mechanical measurements in the shear sandwich geometry were conducted using a Rheometrics RSA2 solids analyzer. This apparatus has been used to determine the order−disorder transition temperatures of the neat diblock copolymers. Dynamical mechanical measurements in the parallel-plate geometry were conducted with a Rheometrics RMS800 mechanical spectrometer. During the measurements, the samples were kept in a temperature-controlled nitrogen atmosphere in order to prevent degradation.

**$\chi$ Parameter.** The values of the experimental Flory−Huggins interaction parameter $\chi$ have already been published in a previous paper.[12] The polymers for which $\chi$ was determined were PS−PI-1, PS−PI-2, PS−PI-4 and PI−PEO-1, PI−PEO-2, PI−PEO-3, and a number of homopolymer blends and diblock copolymers were used to determine $\chi_{PS-PEO}$. We consequently used the Flory−Huggins and Leibler mean-field theories since we analyze the phase boundaries using the random phase approximation for diblock copolymer blends. The conditions for the spinodal point for symmetric homopolymer blends or symmetric diblocks lead to $\chi = 2/N$ and $\chi = 10.5/N$, respectively. (For asymmetric diblock copolymers, a more precise value in place of 10.5 was calculated after ref 16.) The degree of polymerization was calculated using a common segment volume of 70.5 $cm^3$/mol,[17] which was calculated from the molar mass and the average density at 413 K. For an overview more experimental interaction parameters are collected in Figure 2 and are compared to the previous fits. The two "stray" $\chi$ values of the PS−PI-6 and the PI−PEO-4 polymers deviate by about 20% from the previously found values (Figure 2). This might result from an uncertainty in the molar mass determination.

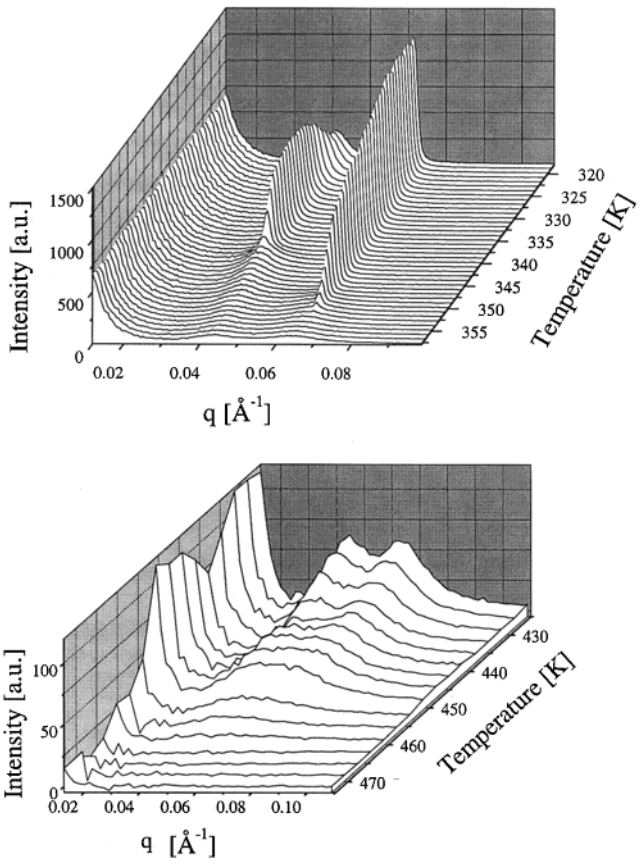


**Figure 3.** Extractions of a SAXS heating/cooling ramp experiment of the $f = 0.5$, $\Phi = 0.5$ sample, which was taken in between 298 K−473 K−298 K with a ramp rate of 10 K/min. A 1 min waiting period was programmed at the maximum temperature of 473 K. The shown extractions result from the heating run. Part (a) shows the two independent sudden decreases of the peak intensities. At the same time the peak width increases and therefore indicates a microphase separation temperature. Part (b) displays the merging of the two correlation peaks and the decay of the scattered intensity at low scattering vectors. The scattered intensity of the waiting period at 473 K was used for background subtraction.

For the calculations of phase diagrams within the random phase approximation we used the measured $\chi$ parameters for the PS−PI and PI−PEO diblock copolymers and the PS/PEO homopolymer blend. The reason for choosing this combination of diblock copolymers and homopolymer blends lies in the influence of the block junction on $\chi$.[18,19] Whereas in the final PS−PI/PI−PEO blend we have to take junction effects of the PS−PI and PI−PEO into account, the interaction between PS and PEO takes place on different chains.

## Results

**SAXS.** The first SAXS experiments were discussed in a previous work.[12] Here we combined small-angle neutron and X-ray scattering experiments of the samples with the copolymer composition $f = 0.5$. We showed that the experimental phase diagram is dominated by the macrophase separation, and the two separated phases order independently. The ordering is indicated by a sudden decrease of the peak intensity and width (Figure 3a and ref 12). Furthermore, we observed that the two correlation peaks of the two disordered phases merge upon heating approximately at the temperature where the low-angle scattering intensity drops. An example is presented in Figure 3b. The small-angle scattering below $q = 0.02$ Å$^{-1}$ is obscured by the beam stop. Two peaks can be clearly identified at 425 K, and the small-angle scattering is large. In the range from 440 to 450 K the two peaks merge, and the merged peak intensity drops suddenly at 453 K. At this temperature the small-angle scattering strongly decreases as well.

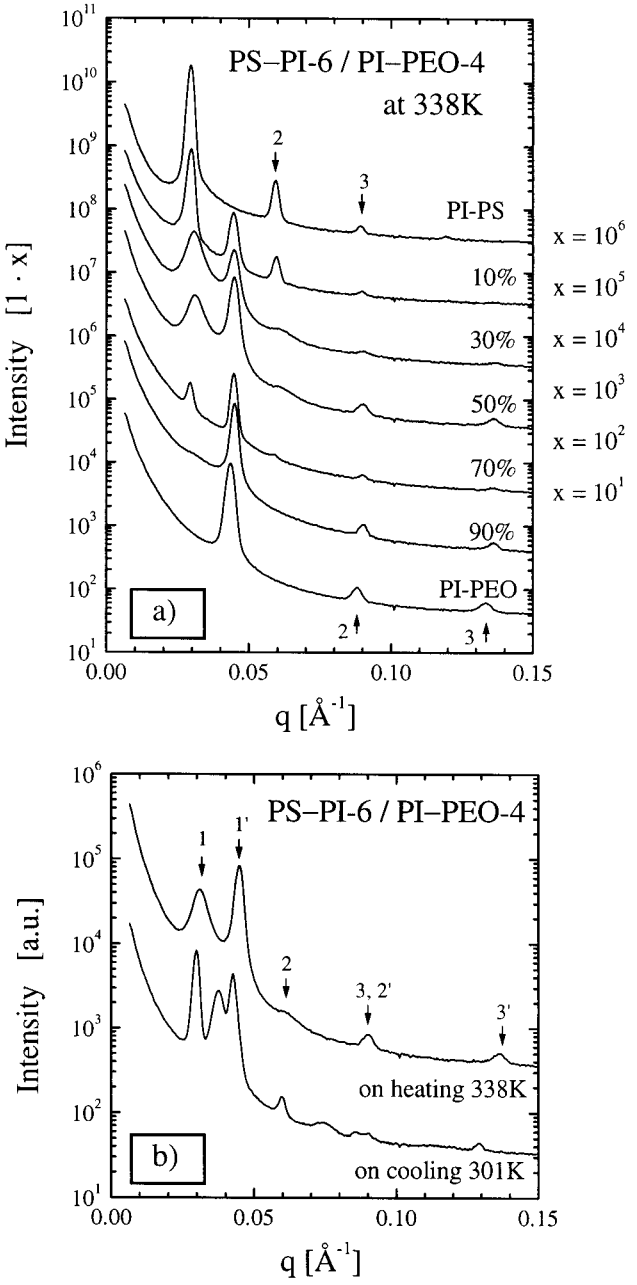


**Figure 4.** (a) Scattered intensity of the PS−PI-6/PI−PEO-4 blend at the temperature 338 K. Several compositions are presented in a semilogarithmic plot. The spectra with lower PI−PEO content are shifted upward. The spectra result from a heating/cooling ramp experiment, which was taken in between 298 K−493 K−298 K with a ramp rate of 10 K/min. A 1 min waiting period was programmed at the maximum temperature of 493 K. For a better statistic 11 spectra were averaged in the range 333−343 K. (b) Comparison of two SAXS spectra of a PS−PI-6/PI−PEO-4 blend with the composition $\Phi = 0.5$. The spectra were taken on the heating run at 338 K and after the cooling at 301 K. The additional shoulder in between the first two peaks results from the crystallinity of the PEO block. Again, the spectra result from an averaging of 11 single taken spectra.

In Figure 4a the scattering of the blend containing diblocks with $f = 0.6$ is depicted for different compositions at 338 K. Considering the first two peaks only, the intensity of the peak at the lower scattering vector

$q^* = 0.0307$ Å$^{-1}$ reduces upon lowering the PI−PS content, and vice versa the peak at $q^* = 0.0446$ Å$^{-1}$ reduces upon lowering the PI−PEO content. This behavior is consistent with a window of two ordered phases coexisting in the phase diagram. The two peaks are then the primary scattering peaks of the PS−PI- and PI−PEO-rich phase.

The peaks at higher scattering vectors reflect the structure of the phases. The higher-order peaks of the blend are correctly indexed with $nq^*$, with $q^*$ being the wavenumber of the first-order peak of either the PS−PI- or PI−PEO-rich phase. This means that two lamellar structures coexist. A possible indexing of all peaks with a $q^*\sqrt{n}$ relation ($n$ being a natural number) is not found to be appropriate, as discussed in detail for the even more complicated case of blends with $f = 0.7$.

When comparing the scattering profile obtained on heating (338 K) with that obtained on cooling (301 K), an additional peak is seen between the two first peaks (Figure 4b). As discussed before,[14,20] the crystallinity of the PEO block can cause stretching of some domains. Further higher-order reflections are caused by the third phase, which contains the crystalline PEO.

For the PS−PI-4/PI−PEO-3 blends with the volume fraction $f = 0.7$ the scattering curves are presented in Figure 5a. The data represent the state after cooling to a temperature of 301 K and are not influenced by crystallization (when compared to higher temperatures). The two first peaks at $q^* = 0.0280$ Å$^{-1}$ and $q^* = 0.0388$ Å$^{-1}$ behave similarly as a function of composition as already discussed for the blend of diblocks with $f = 0.6$. It should be mentioned that the peak at $q^* = 0.0280$ Å$^{-1}$ disappears for PI−PEO compositions $\Phi = 0.8$ and above. In this range the two diblock copolymers seem to be miscible, forming a single ordered phase.

The pure PS−PI-4 sample has higher-order reflections at relative positions of $\sqrt{2}$, $\sqrt{3}$, $\sqrt{7}$, and $\sqrt{9}$, which are typical for a body-centered-cubic symmetry. In this structure the PS-block would form spheres in a PI-matrix. In ref 21 this structure was not reported on the high $f$ value range but is likely to be found. The pure PI−PEO-3 sample has higher-order reflections at relative positions of $\sqrt{3}$, $\sqrt{4}$, $\sqrt{7}$, and $\sqrt{9}$. Because of the missing reflection at $\sqrt{2}$, the ordered structure is likely to be hexagonally packed cylinders.

The Bragg peaks observed in the blends of two phases are combinations of higher-order reflections (Figure 5b). This means that two ordered phases coexist, and both the PS−PI- and PI−PEO-rich phases remain in the same unchanged structure compared to the pure phases. Nonetheless, one could argue that all peaks could be indexed after the first peak at $q^* = 0.0280$ Å$^{-1}$. Peaks are found at multiples $\sqrt{2}$, $\sqrt{3}$, $\sqrt{6}$, $\sqrt{7}$, $\sqrt{8}$, $\sqrt{14}$, and $\sqrt{18}$ of $q^*$. But, a possible simple cubic symmetry does not produce a peak at the relative position $\sqrt{7}$ (since there are no $h^2 + k^2 + l^2 = 7$), and in a body-centered-cubic structure there would be no peak at the relative position $\sqrt{14}$. Neither a face-centered-cubic structure is very likely, because a peak at a relative position $\sqrt{8/3}$ is not found. For the two-phase coexisting system with $f = 0.6$ and 0.7, the possible common peak indexing might result from an adjustment of the $d$ spacing of the two phases due to a large interfacial area between the domains. Furthermore, the finite miscibility of the two polymers makes the change of the peak positions more likely.

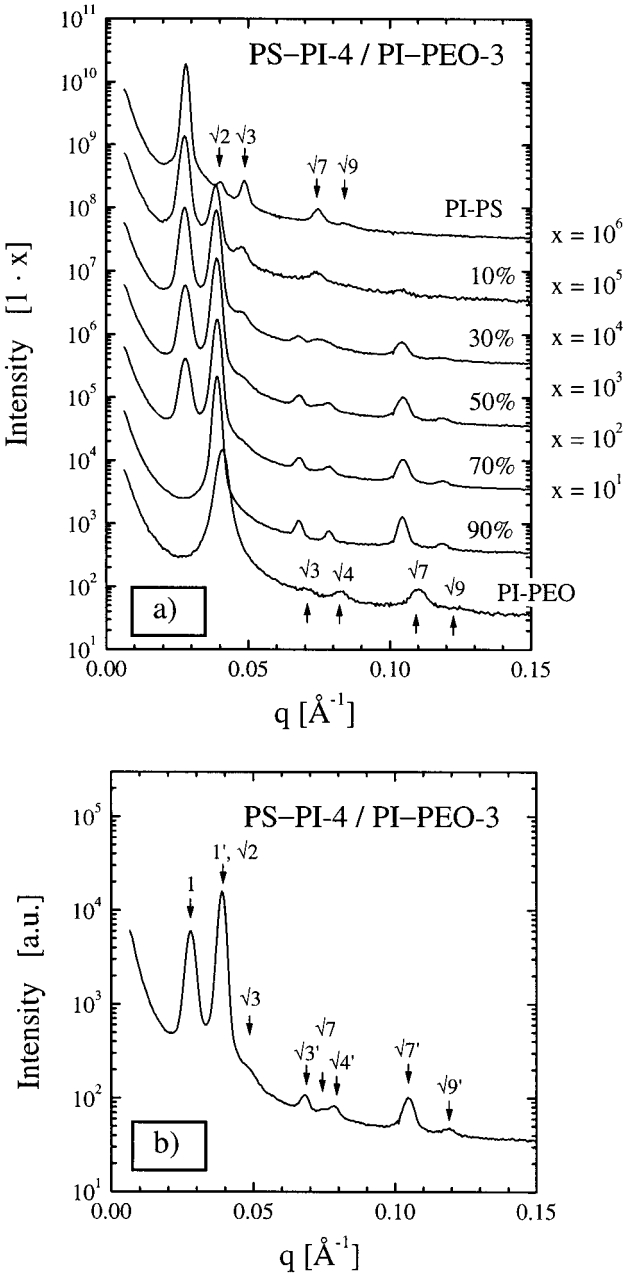


**Figure 5.** (a) Scattered intensity of the PS−PI-4/PI−PEO-3 blend at the temperature 301 K after the cooling run. Several compositions are presented in a semilogarithmic plot. The spectra with lower PI−PEO content are shifted upward. The spectra result from a heating/cooling ramp experiment, which was taken in between 298 K−503 K−298 K with a ramp rate of 10 K/min. A 1 min waiting period was programmed at the maximum temperature of 503 K. The spectra result from an averaging of 11 single taken spectra. (b) Indexing of the SAXS spectrum of a PS−PI-4/PI−PEO-3 blend with the composition $\Phi = 0.5$. The peak positions are related to the two first peaks, which result from the PS−PI- and PI−PEO-rich phases.

The peak positions of the first two peaks of the $f = 0.7$ system can be followed well in Figure 5a. The peak position of the first peak (of the PS−PI-rich phase) is not influenced by the composition, whereas the peak position of the second peak (of the PI−PEO-rich phase) changes between the pure PI−PEO and the 90% PI−PEO samples and stays constant for all other compositions. This behavior is another hint for a single ordered phase above 80% PI−PEO-3 and for the coexistence of two phases below 80%. For the $f = 0.6$ system

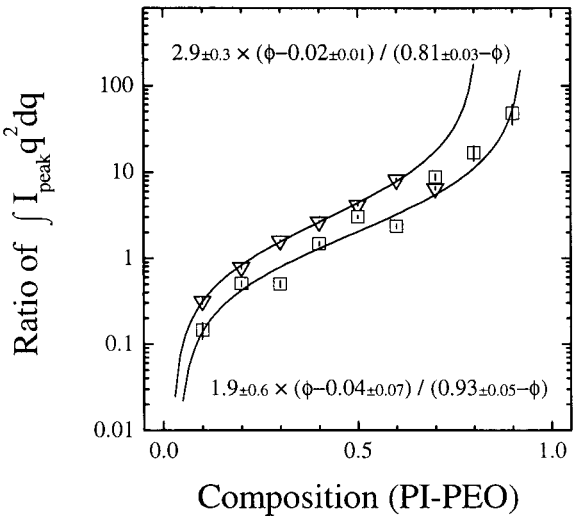


**Figure 6.** Ratio of the integral peak intensity of the two first peaks vs the composition for the PS−PI-1/PI−PEO-1 (□) and the PS−PI-4/PI−PEO-3 (▽) blends. The dependence is described with the written equations and further discussed in the text.

(Figure 4a) the peak positions are slightly elevated in the composition range of 30%−90% PI−PEO, which is due to the finite miscibility of the two separate phases. The detailed reason for elevated $q$ values cannot be given in this study.

From the peak width the long-range order dimension $L$ can be calculated after $L = \lambda/(\beta_S \cos\theta)$,[23] with $\lambda$ being the wavelength of the X-ray beam, $\beta_S$ being the full width at a half-maximum intensity, and $2\theta$ being the scattering angle. From the peak widths of the $f = 0.7$, $\Phi = 0.5$ blend (0.0036, 0.0027 Å$^{-1}$), the long-range order dimension is estimated to be $L = 420$ Å (±1%) and 560 Å (±3%) for the PS−PI- and PI−PEO-rich phases, respectively. The different values indicate two phases as well.

We have calculated the two integrals corresponding to the second moment of the intensities of the peaks at $q^*$ for PS−PI-1/PI−PEO-1 and PS−PI-4/PI−PEO-3 blends, which should be proportional to the amount of the PI−PEO-rich and PS−PI-rich phases, respectively, weighted by the squared contrast and form factor.[22,23] Then we plotted the ratio of the integrals (PI−PEO/PS−PI) vs the composition of PI−PEO (Figure 6). Obviously, the PI−PEO respective peak intensity is growing with the PI−PEO content. The ratio of the integrals $r_I$ is described by a lever rule, according to

$$r_1 = \frac{\int I_{\text{peak}1} q^2 \, dq}{\int I_{\text{peak}2} q^2 \, dq} = A \frac{\Phi - \Phi_2}{\Phi_1 - \Phi} \qquad (2)$$

with $\Phi_1$ being the PI−PEO content of the PI−PEO-rich phase and $\Phi_2$ the PI−PEO content of the PS−PI-rich phase. The prefactor $A$ depends on the squared contrast ratio and the form-factor ratio. The former is calculated to be 2.1, and therefore we roughly expect $A$ to be 2.1; however, the estimation of the form-factor ratio is not straightforward, and deviations from $A = 2.1$ are likely. The actual fits of eq 2 (Figure 6) compare quite well with experiment. The compositions obtained for the two separated phases 0.04/0.93 and 0.02/0.81 for the PS−PI-1/PI−PEO-1 and the PS−PI-4/PI−PEO-3 blends seem to be reasonable. Whereas for the PS−PI-1/PI−PEO-1 blend $A$ is quite close to the expected value of 2.1 (the whole intensity is collected in the first-order reflection and higher-order peaks are missing[12]), the PS−PI-4/PI−PEO-3 blend shows a distinctively larger $A$. This might be due to the PI−PEO-rich phase containing some amount of PS−PI.

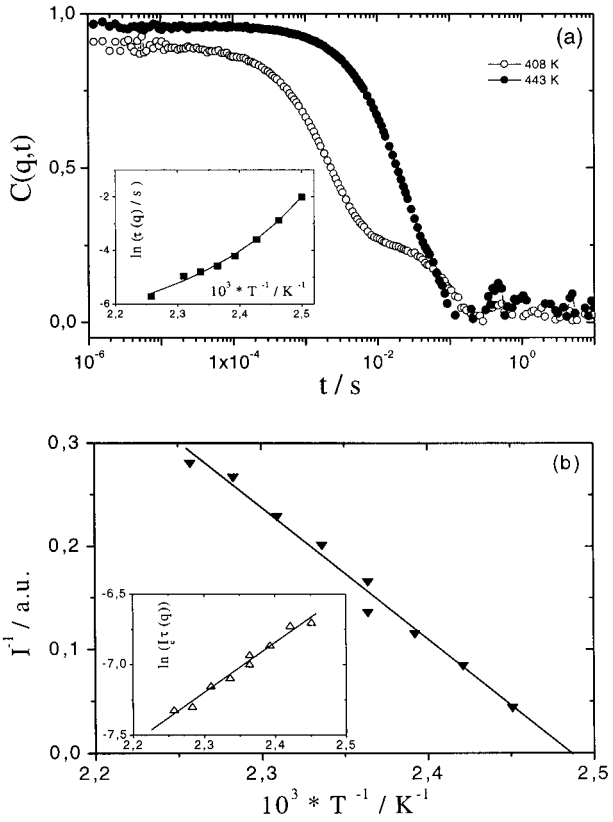


**Figure 7.** (a) Intermediate scattering function $C(q,t)$ of the PS−PI-1/PI−PEO-1 blend with 0.7 volume fraction in PI−PEO at $q = 0.027$ nm$^{-1}$ and two temperatures in the homogeneous regime. The single interdiffusion time $\tau(q)$ for the relaxation of concentration fluctuations is shown in the Arrhenius plot of the inset. (b) Light scattering intensity $I_c$ associated with the concentration fluctuations in this blend presented as a mean-field plot $I_c^{-1}$ vs $T^{-1}$ that leads to the spinodal temperature $T_s = 403$ K. The purely kinetic factor $\tau(q)$. $I_c$ shows now the expected Arrhenius $T$ dependence (cf. inset of a).

**PCS.** Figure 7a displays the experimental dynamic structure factor of the PS−PI-1/PI−PEO-1 blend with $\Phi$(PI−PEO) = 0.7 at low $q$ (=0.03 nm$^{-1}$) for two temperatures in the homogeneous phase. At high temperatures, $C(q,t)$ has a bimodal exponential shape due to fast interdiffusion[24] and a slow cluster diffusion. Approaching the macrophase separation temperature, the interdiffusion process is expected to be the dominant mechanism in $C(q,t)$. The interdiffusion time $\tau(q) = (Dq^2)^{-1}$ ($D$ being the interdiffusion coefficient) at $q = 0.027$ nm$^{-1}$ increases rapidly with decreasing temperature. Despite the fact that this blend is far above its glass transition, the observed temperature dependence of $\tau(q)$ is clearly stronger than Arrhenius (inset of Figure 7a) due to the unfavorable thermodynamic interactions. The latter are directly reflected in the intensity $I_c$ shown in Figure 7b. In fact, the product $I_c\tau(q)$ which is of purely kinetic nature (lower inset) displays the expected Arrhenius temperature dependence with a physically meaningful activation energy (~29 kJ/mol). In the mean-field theory, the divergence of $I_c^{-1}$ defines the spinodal temperature $T_s$ = 403 K. Further, the

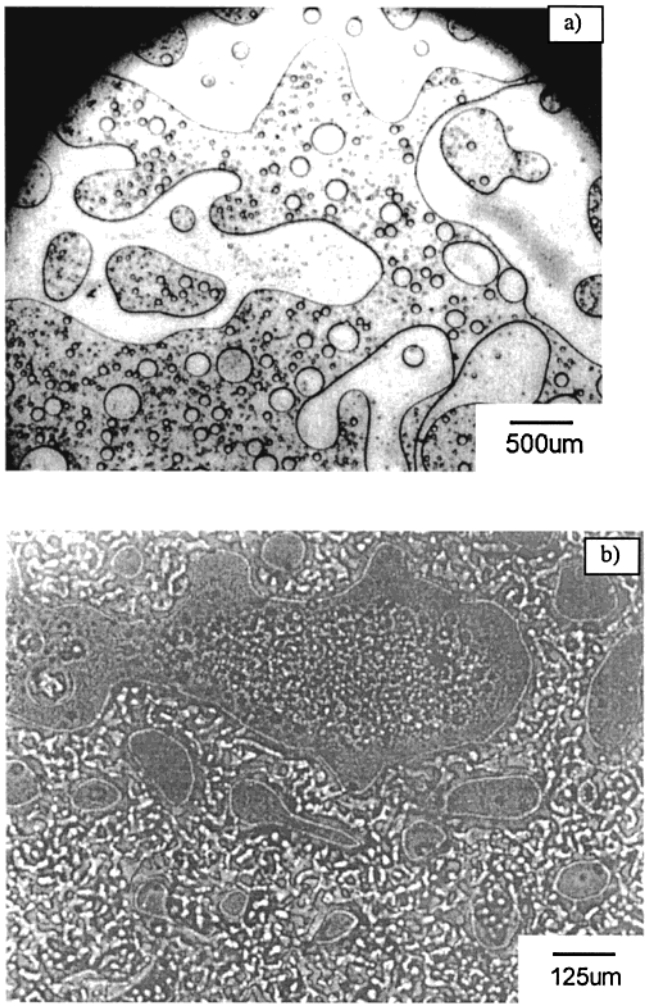


**Figure 8.** (a) Light microscopy of a PS−PI-4/PI−PEO-3 blend with the composition $\Phi = 0.5$ at 523 K. The domains of sizes between ≈50 and ≥1000 $\mu$m are observed. (b) Light microscopy of a PS−PI-4/PI−PEO-3 blend with the composition $\Phi = 0.5$ at 298 K after heating to 523 K. Domains of about 50 $\mu$m were already present at 523 K. The smaller domains could be only resolved at room temperature when the hot stage was removed.

macrophase separation was confirmed visually documented by clouding which occurred below 407 K for this blend.

**LM.** The samples at low temperatures look quite turbid without any structure visible by light microscopy. It should be mentioned that these samples are yielded by the solvent casting process. Upon heating, the samples become liquid and begin to flow, and domains can be identified; see for example Figure 8a, which shows a micrograph for PS−PI-4/PI−PEO-3. Upon cooling, the domains stay nearly unchanged. However, at a higher magnification further domains can be identified within the already existing domains. The large domain in the top half of Figure 8b is surrounded by a bright and dark line, which indicates that this domain is rich in the optically denser PS−PI. This large domain nevertheless contains smaller domains which are PI−PEO-rich. Conversely, the surrounding PI−PEO-rich phase contains many PS−PI-rich phases.

Domains within domains have been reported for quick cooling processes,[25,26] when the blend is dynamically asymmetric. Here the PS-rich phase forms a sponge phase for intermediate times, which forms more compact shapes after longer periods of time. We would classify the observed structures of the PS−PI-rich phase to be in late stage.

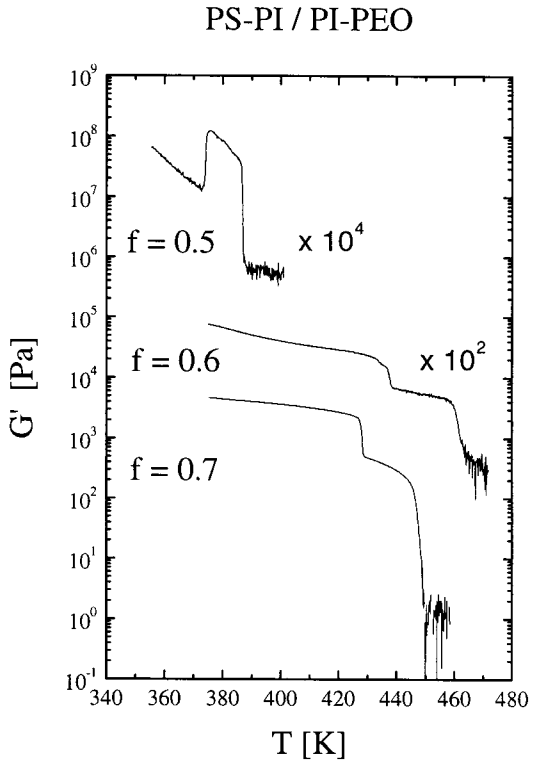


**Figure 9.** Dynamical mechanical elastic moduli as a function of temperature for the blends PS−PI-1/PI−PEO-1 ($f = 0.5$), PS−PI-6/PI−PEO-4 ($f = 0.6$), and PS−PI-4/PI−PEO-3 ($f = 0.7$). The conditions were $\omega = 5$ rad/s; $\gamma_0 = 4\%$, cooling rate 1 K/min, parallel plate geometry (RMS800).

**Rheology.** The elastic modulus of three samples with different chain length ratios $f = 0.5$, 0.6, and 0.7 is shown in Figure 9 as a function of temperature. The composition of all samples is $\Phi = 0.5$, and all experiments were conducted upon cooling from high temperatures. Below an elastic modulus of 20 Pa, the two-plate shear geometry becomes less sensitive and the data are noisy. The sharp decrease of the elastic modulus indicates an order−disorder transition of a phase which is ordered below $T_{ODT}$ and disordered above $T_{ODT}$.

The blend of diblocks with $f = 0.7$ shows two distinct order−disorder transition temperatures at 446 and 427 K. The sample with $f = 0.6$ shows two clear order−disorder transition temperatures at 460 and 437 K as well. The corresponding heating ramp experiments showed the same behavior with a hysteresis of about 7 K. The sample with $f = 0.5$ shows one clear order−disorder transition at 386 K. At 374 K another phase transition is found. In comparison to the SAXS experiments, we expect another order−disorder transition, and the lower elastic modulus at low temperatures must be due to rearrangements or orientation of the domains (shear thinning).

## Discussion

The experimental phase diagrams from the SAXS experiments are listed in Figures 10a−c. The previously published phase diagram[12] of the PS−PI-1/PI−PEO-1 blend with a diblock composition $f = 0.5$ (Figure 1a) contains the one-phase, disordered state at high temperatures. The binodal of phase separation was observed

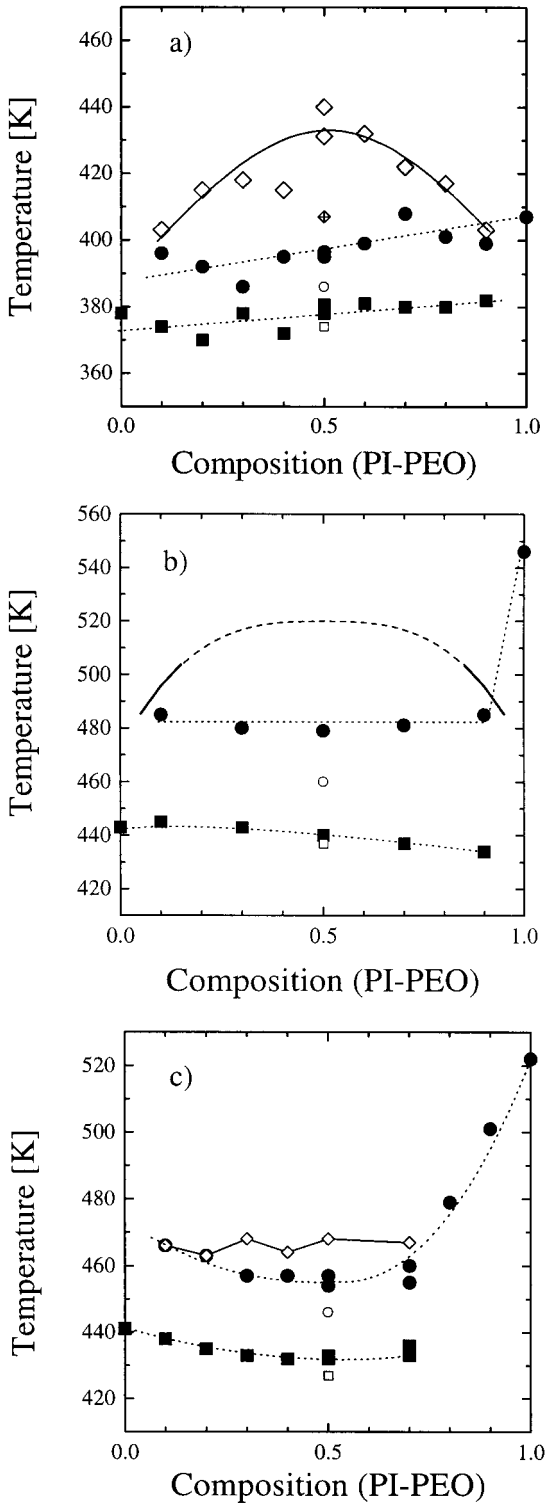


**Figure 10.** Phase diagram of the PS−PI-1/PI−PEO-1 blend with a chain length ratio of $f = 0.5$ (a), 0.6 (b), and 0.7 (c). Depicted are the binodal of macrophase separation (◇) and microphase separation temperatures of the PI−PEO-rich phase (●) and the PS−PI-rich phase (■) from SAXS measurements as a function of composition. The dotted lines are a guide for the eye of the two microphase separation boundaries. The solid line is a guide for the eye of the binodal of macrophase separation. The dashed extension in (b) just demonstrates that higher temperatures were not accessible. For comparison, we added the bimodal of LS experiments (crossed ◇) and the microphase separation temperatures of the PI−PEO-rich phase (○) and the PS−PI-rich phase (□) from rheology measurements.

in the temperature range 400−440 K. Below, two independent order−disorder transition temperatures were observed. The PI−PEO-rich phase orders at temperatures of 390−410 K, and the PS−PI-rich phase orders at temperatures of 370−380 K. Thus, this phase diagram is dominated by macrophase separation, as predicted by the random phase approximation (Figure 1a). The phase boundaries agree semiquantitatively.

The phase diagram of the PS−PI-6/PS−PEO-4 blend with $f = 0.6$ is similar to that for the blend of symmetric diblocks (Figure 10b); the binodal of phase separation was not observed. The two distinct order−disorder transition temperatures speak for a phase-separated system with a PS−PI-rich and a PI−PEO-rich phase. Therefore, the qualitative behavior is still dominated by macrophase separation (like Figure 10a).

The phase diagram of the PS−PI-4/PI−PEO-3 blend with the diblock composition $f = 0.7$ shows order−disorder-transitions for $\Phi > 0.8$ (Figure 10c). Within the main composition range ($0.1 \geq \Phi \geq 0.8$) the binodal of macrophase separation is found close to the two order−disorder transition temperatures. The phase diagram has therefore either a microphase- or macrophase-separation dominated range. In comparison to theory, the balance of macrophase and microphase separation takes place for different PI compositions $f$. Whereas experimentally we expect a Lifshitz point around $f \approx 0.7$, the theoretical prediction was around $f \approx 0.6$. This slight discrepancy might be due to small errors in the experimental $\chi$ interaction parameters. However, the general trend of a suppressed macrophase separation phase boundary is described correctly by the theory.

The phase diagrams discussed above were measured by SAXS. The other methods (light scattering, rheology) gave qualitatively similar results, although with some differences (typically 10−20 K) in phase transition temperatures. Since all phase diagrams presented here are mainly governed by macrophase separation, we compare the behavior of a two-phase system under different conditions. Under these conditions the domain size and maybe even the composition in either phase might vary, and therefore, it cannot be expected that all methods give exactly the same temperatures.

## Summary

Several PS−PI/PI−PEO diblock copolymer blends were investigated by SAXS, LS, LM, and rheology. The increase of the PI composition, $f$, in either block copolymer increased the miscibility of the two polymers, but within our experimental limit $f \leq 0.7$, we find mainly a macrophase separation dominated phase diagram. Only at $f = 0.7$ the microphase separation begins to come into play, in the vicinity of which we expect a Lifshitz point. Here ($f = 0.7$) at the best miscibility, domains within domains were observed by LM. This structure explains large interfacial area between the domains, which could lead to an adjustment of the $d$ spacing of the two phases likely. The alignment of microphase-separated phases imposed by the large interfacial area might be another indication for the vicinity of a Lifshitz point.

**Acknowledgment.** We gratefully thank the European Program "Training and Mobility of Researchers", which financed H.F., N.H., L.M., L.C., D.D., and R.S. through the CAPS project: "Complex Architectures in diblock copolymer based Polymer Systems". Beamtime at Daresbury was provided by the EPSRC through the materials SESS.

## References and Notes


(1) Hamley, I. W. *The Physics of Block Copolymers*; Oxford University Press: Oxford, 1998.
(2) Hashimoto, T.; Yamasaki, K.; Koizumi, S.; Hasegawa, H. *Macromolecules* **1993**, *26*, 2895.
(3) Hashimoto, T.; Koizumi, S.; Hasegawa, H. *Macromolecules* **1994**, *27*, 1562.
(4) Koizumi, S.; Hasegawa, H.; Hashimoto, T. *Macromolecules* **1994**, *27*, 4371.
(5) Yamaguchi, D.; Shiratake, S.; Hashimoto, T. *Macromolecules* **2000**, *33*, 8258.
(6) Kane, L.; Satkowski, M. M.; Smith, S. D.; Spontak, R. J. *Macromolecules* **1996**, 29, 8862.
(7) Lin, E. K.; Gast, A. P.; Shi, A.-C.; Noolandi, J.; Smith, S. D. *Macromolecules* **1996**, *29*, 5920.
(8) Papadakis, C. M.; Mortensen, K.; Posselt, D. *Eur. Phys. J. B* **1998**, *4*, 325.
(9) Kimishima, K.; Jinnai, H.; Hashimoto, T. *Macromolecules* **1999**, *32*, 2585.
(10) Olmsted, P. D.; Hamley, I. W. *Europhys. Lett.* **1999**, *45*, 83.
(11) Ijichi, Y.; Hashimoto, T. *Polym. Commun.* **1988**, *29*, 135.
(12) Frielinghaus, H.; Hermsdorf, N.; Almdal, K.; Mortensen, K.; Messé, L.; Corvazier, L.; Fairclough, J. P. A.; Ryan, A. J.; Olmsted, P. D.; Hamley, I. W. *Europhys. Lett.* **2001**, *53*, 680.
(13) Ndoni, S.; Papadakis, C.; Bates, F. S.; Almdal, K. *Rev. Sci. Instrum.* **1995**, *66*, 1090.
(14) Ebel, H. F.; Luttrighaus, A. In *Houben Weyl XIII/I*; Verlag: Stuttgard, 1970.
(15) Bras, W.; Derbyshire, G. E.; Devine, A.; Clarke, S.; Cooke, J.; Komanschek, B. U.; Ryan, A. J. *J. Appl. Crystallogr.* **1995**, *28*, 26.
(16) Leibler, L. *Macromolecules* **1980**, *13*, 1602.
(17) Rosedale, J. H.; Bates, F. S.; Almdal, K.; Mortensen, K.; Wignall, G. D. *Macromolecules* **1995**, *28*, 1429.
(18) Frielinghaus, H.; Abbas, B.; Schwahn, D.; Willner, L. *Europhys. Lett.* **1998**, *44*, 606.
(19) Frielinghaus, H.; Pedersen, W. B.; Larsen, P. S.; Almdal, K.; Mortensen, K. *Macromolecules* **2001**, *34*, 1096.
(20) Ryan, A. J.; Fairclough, J. P. A.; Hamley, I. W.; Mai, S.; Booth, C. *Macromolecules* **1997**, *30*, 1723.
(21) Khandpur, A. K.; Förster, S.; Bates, F. S.; Hamley, I. W.; Ryan, A. J.; Bras, W.; Almdal, K.; Mortensen, K. *Macromolecules* **1995**, *28*, 8796.
(22) Lovesey, S. W. *Theory of Neutron Scattering from Condensed Matter*; Oxford University Press: Oxford, 1984.
(23) Evmenenko, G.; Theunissen, E.; Mortensen, K.; Reynaers, H. *Polymer* **2001**, *42*, 2907.
(24) Beiner, M.; Fytas, G.; Meier, G.; Kumar, S. *Phys. Rev. Lett.* **1998**, *81*, 594.
(25) Gutmann, J. S.; Müller-Buschbaum, P.; Stamm, M. *Faraday Discuss.* **1999**, *112*, 285.
(26) Tanaka, H. *Phys. Rev. Lett.* **1996**, *76*, 787. Tanaka, H. *Phys. Rev. E* **1995**, *51*, 1313.


MA010233Q